Binder-free Wood Converted Carbon for Enhanced Water Desalination Performance

Rui He[1], Manish Neupane[2], Akhter Zia[2], Xiaozhou Huang[1], Crystal Bowers[1], Jun Lu[3,4], Yingchao Yang[2,]*, Pei Dong[1,]**

R. He, X. Huang, C. Bowers, P. Dong

Department of Mechanical Engineering, George Mason University, 4400 University Drive, Fairfax, VA 22030, USA

Email: pdong3@gmu.edu

M. Neupane, A. Zia, Y. Yang

Department of Mechanical Engineering, University of Maine, 168 College Ave, Orono, ME 04469, USA

Email: yingchao.yang@maine.edu

J. Lu

Chemical Sciences and Engineering Division, Argonne National Laboratory, 9700 South, Cass Avenue, Lemont, IL 60439, USA

College of Chemical and Biological Engineering, Zhejiang University, Hangzhou 310027, China.

Email: junzoelu@zju.edu.cn

Keywords: binder-free, wood, chemical activated carbon, water desalination, sustainability

Abstract

The design and synthesis of high-performance and economical carbon electrode play a critical role in developing energy-efficient water desalination technologies. As a sustainable approach, the low-cost and abundant biomass materials are promising candidates to prepare porous carbon for capacitive deionization. In this work, the binder-free porous carbon sheets have been successfully prepared using natural balsa, pine, and bass wood by thermal carbonization and treated by chemical activation. The carbon electrode materials converted from balsa and pine exhibit a comparable salt adsorption performance by capacitive deionization due to the extensive surface area, substantial electrical property, and superior hydrophilic performance. The following activation treatment on balsa converted carbon further enhances the surface and electrical properties and benefits the

desalination performance. The salt adsorption capacity of the activated balsa electrode exhibits 12.45mg g^{-1}. Additionally, 19.52 mg g^{-1} Pb^{2+} and 20.06 mg g^{-1} Cr^{3+} heavy metal adsorption capacity is also observed with activated balsa electrode in 100 mg L^{-1} $PbCl_2$ and 50 mg L^{-1} $CrCl_3$, respectively. To the best of our knowledge, this is so far the highest NaCl adsorption capacity performance by using pure wood converted carbon as electrode, and these promising results indicate that activated balsa is an extraordinary material for water desalination.

1. Introduction

Currently, plants take ~82.4% of overall biomass with ~545.8 gigatons on Earth.[1] Among them, approximately 258 - 340 million available biomass have been generated annually.[2] As a green approach, tremendous research efforts have been made to convert the biomass to advance functional materials in different areas, such as supercapacitor, batteries, gas adsorption, water purification.[3–6] Taking advantage of the specific pore-size distribution, abundant, economical, and environmentally-friendly features, biomass converted carbon is gaining exaggerated attention.[7] As biomass precursor, the peel of fruits, including pomelo, watermelon, citrus; eggplant, tea, and xylose have been successfully carbonized to prepare biomass converted porous carbon.[8–13] The carbon film preparation usually consists of thermal carbonization and carbon powder-binder mixture, along with activation to create auxiliary porous structures.[9] It is noticeable that the original unique organic structure will be demolished when pulverizing the biomass converted carbon into powder. Meanwhile, the addition of a non-conducting polymer binder will dramatically lower the specific surface area (SSA) and conductivity of the porous carbon.[9,14,15] Thus, in order to simplify the preparation process while maintain the unique internal structure and properties, the binder-free carbon film needs to be designed with deliberately selected natural porous precursor, treated with tuned parameters, and further be applied in, for example, water desalination area.

Water desalination is a technique that can expel the harmful ions from water. The technological advancement includes multi-stage flash, electrodialysis, and reverse osmosis.[16–18] However, high energy consumption, low efficiency and membrane fouling challenge their massive utilization.[19] Among all these techniques, capacitive deionization (CDI) for water desalination is considered to be an energy-efficiency technique and has attracted researchers' enthusiasm, as it takes

ions/chemicals out of water instead of taking water out. It is also commonly considered an environmentally friendly, economical, and easy-operate technique.[20–23]

CDI executes the electrosorption to remove the ions by ingesting them into a pair of charged porous carbon electrodes: Once the voltage (typical 1.0V-1.6V) is afforded, the ions inside brackish water will move towards the electrode that incorporates reversed charge, forming an electric double layer (EDL) between the interface of the electrode and brackish solution.[20,24,25] In general, high SSA and conductivity of the electrode materials could dramatically improve water desalination performance.[26]

Herein, to design an advanced binder-free biomass converted carbon for CDI as a sustainable approach, we reported three species of common wood: balsa, pine and bass as precursor to prepare porous carbon films. The wood converted carbon is expected to maintain its natural wood porous structure, ensuring a large SSA and excellent electrical properties. The electrodes performed the electrosorption in sodium chloride (NaCl) solution with a voltage provided (**Figure 1**). Seeking for an enhanced desalination performance, we further used potassium hydroxide (KOH) as an activating agent. The chemical activation occurs at a high temperature to generate extra pore structures on the wood converted carbon through the reaction between KOH and carbon to further increase SSA to enhance water desalination performance. The NaCl and heavy metal ions adsorption performance of activated samples have also been conducted.

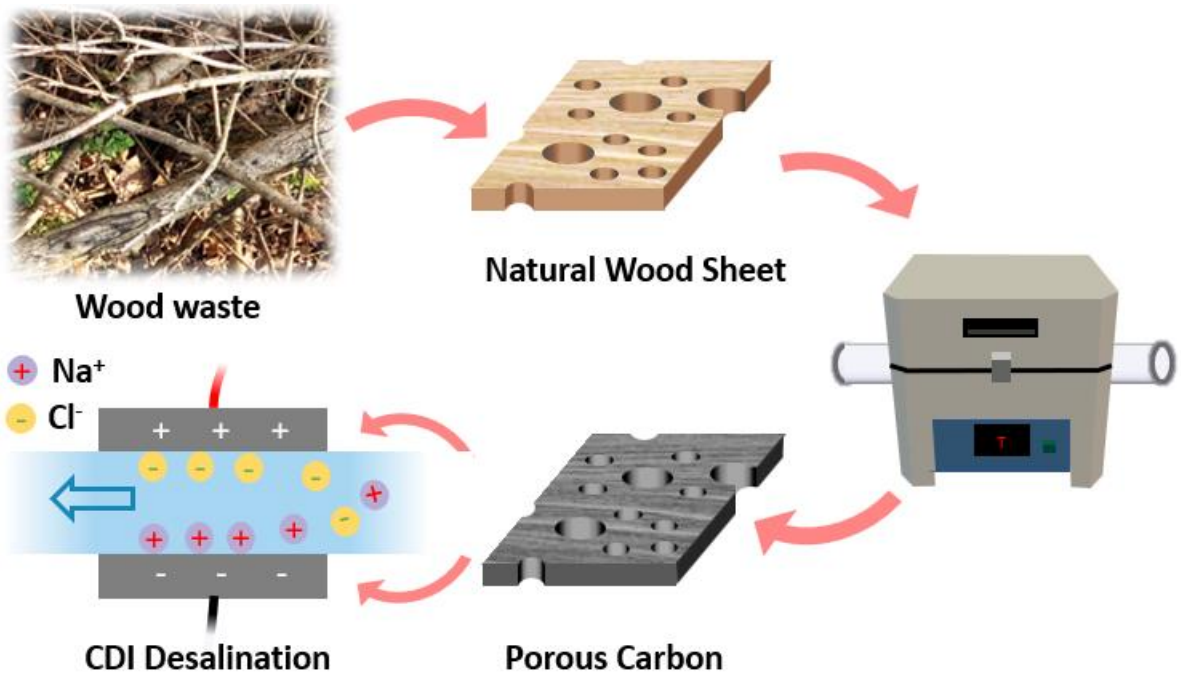

Figure 1. Schematic illustration of wood converted carbon preparation and its application CDI for water desalination

2. Results and Discussion

To systematically study the role of binder-free wood converted carbon in CDI, three carbon sheets were synthesized and named as carbonized balsa, carbonized pine and carbonized bass to represent different natural wood precursors. It has been proved the activating agent, KOH will react with carbon above 600 ºC following the equation below: [27,28]

$$6KOH+2C \rightarrow 2K+3H_2+2K_2CO_3 \quad (1)$$

$$K_2CO_3+2C \rightarrow 2K+3CO \quad (2)$$

In order to obtain the samples with fully reaction between KOH and carbon, the KOH activated wood converted carbon samples are prepared under 700ºC and named as activated balsa and activated pine.[29,30] AC carbon film was prepared as a benchmark group. The surface properties, including surface morphology, surface hydration and SSA, and electrical properties have been investigated. The NaCl adsorption has been performance with a single-pass mode setup while heavy metal adsorption with a batch mode, which is consistent with other's work.[31] The results

of surface and electrical test directly affect the salt adsorption performance, which will be discussed in this section.

2.1 Surface properties

2.1.1 Morphology

Optical and SEM images of carbonized wood samples, including balsa (**Figure 2a-e**), pine (Figure 2f-j) and bass wood (Figure 2k-o), were used to observe the surface morphology. Taking printing balsa (Figure 2b) as an example, it exhibits two channel sizes with different pore diameters after carbonization, in which the dominated small channel possesses an approximately 40 μm average pore size with an average channel wall thickness approximately 210 nm according to Figure 2c and e. It is also noticeable that some hollow channels were split by the sheet structure with abundant tiny pores (Figure 2d). Figure 2f-j presents carbonized pine morphology, from which coherent annual rings lines occur in both wood and wood converted carbon samples (Figure 2f, g). The channels apart from annual rings usually have a uniform dispersion (Figure 2h) while the extraordinary structure contrast aside the ring could be easily distinguished (Figure 2i). Additionally, carbonized bass samples manifest porous structures (Figure 2k-o). However, as shown in Figures 2m and n, several channels are entirely obstructed by carbonized organic tissue (red circle), which decreases the porosity of carbonized bass. Due to the particular wood structure, the average channel wall thickness of carbonized pine and carbonized bass is approximately 1.3 μm and 1 μm, respectively, higher than that of carbonized balsa (Figure 2j and o). As shown in **Figure S1**, after activation, a lot of cracks and holes were observed on the surface of both activated balsa and activated pine, which were induced by the reaction of KOH and carbon at high temperatures. However, the natural wood porous structures are largely retained. It is also noticeable that at the position with thick carbon wall (Figure S1b), the surface morphology barely modified after activation. As a comparison group, AC film also shows a porous structure with obvious carbon powder observed (Figure S1). The morphology indicates that each carbonized wood converted carbon sample possesses an exclusive structure analogous to the wood. Typically, the carbon electrode manufacturing consists of grinding the carbon to powder and mixing with polymer binder.[9] In this research, the as-obtained binder-free wood converted carbon electrode can be directly attached to the CDI current collector after the thermal treatment, which largely facilitate the material preparation.

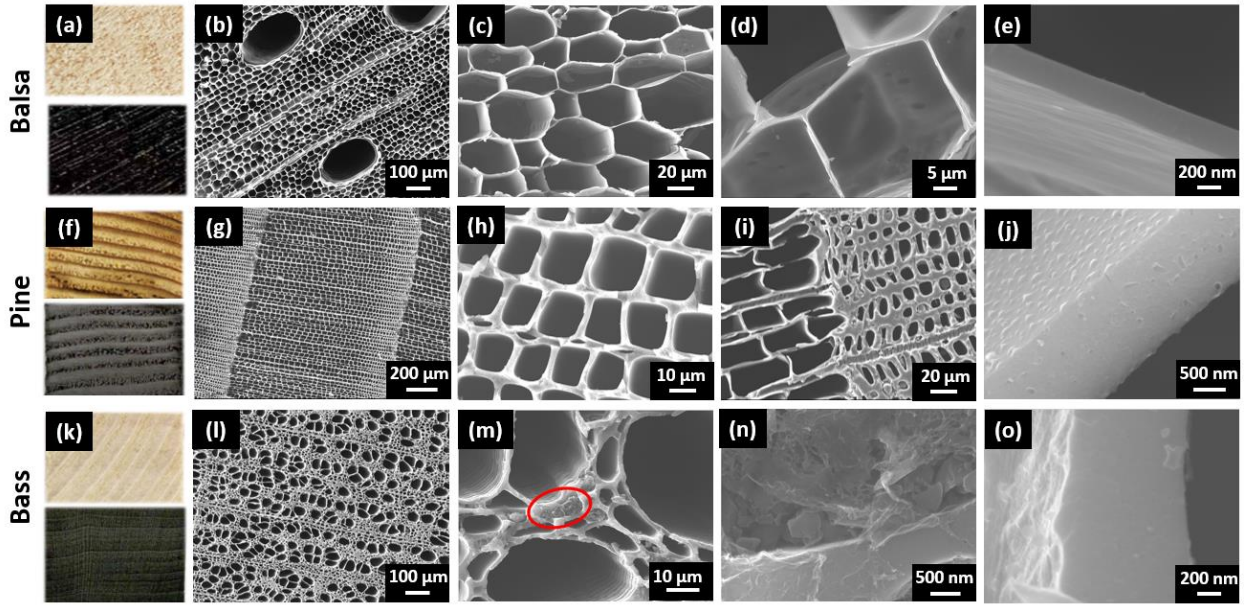

Figure 2. Morphology of wood and wood converted carbon samples. (a) optical image of balsa wood (before carbonization) and carbonized balsa (after carbonization). (b-e) SEM images of carbonized balsa. (f) optical image of pine wood and carbonized pine. (g-j) SEM images of carbonized pine. (k) optical image of bass wood and carbonized bass. (l-o) SEM images of carbonized bass.

2.1.2 Surface hydration

The surface energy determines the adhesion of the liquid to the substrate and the water contact angle reveals the hydration property of the materials.[21] A hydrophilic material implies the liquid can penetrate the material easily and all segments will participate in the deionization process with an agile ion diffuse rate.[21,32] As shown in **Figure 3**, the carbonized balsa, carbonized pine, activated balsa and activated pine show an excellent hydrophilic property as the water droplet is absorbed by the materials within 0.1 s (**Video S1**). Additionally, Ethanol and chloroform perform 0-degree contact angle among both carbonized balsa and pine (**Figure S2**). Therefore, according to Owens, Wendt, Rabel, and Kalble (OWRK) method,[33] the surface energy of carbonized balsa and carbonized pine could reach as high as 82.23 mN m^{-1}. Meanwhile, the activated carbon samples own a similar water contact angle results to carbonized wood. The high surface energy ensures a robust liquid-carbon interaction and largely promotes the wettability of carbonized balsa and pine carbon materials. As a result, the entire carbon electrode will take participate in the desalination when immersing into the NaCl solution.

Both carbonized bass and AC perform a 0 degree ethanol and chloroform contact angle (Figure S2). Meanwhile, carbonized bass also exhibits a hydrophilic surface with a 67.1° water contact angle, leading to 33.96 mN m^{-1} surface energy. This is because binder-free carbonized samples largely preserve the unique morphology of wood, and for carbonized bass, some channel structures are fully blocked by carbonized tissue as shown in Figure 2m (red circle). Additionally, the water contact angle of the AC film is 132.2° with 50.23 mN m^{-1} surface energy. The hydrophobic surface could be explained by the non-channel structure of AC powder and the addition of a hydrophobic PVDF binder, which has been proved by others' work. [34]

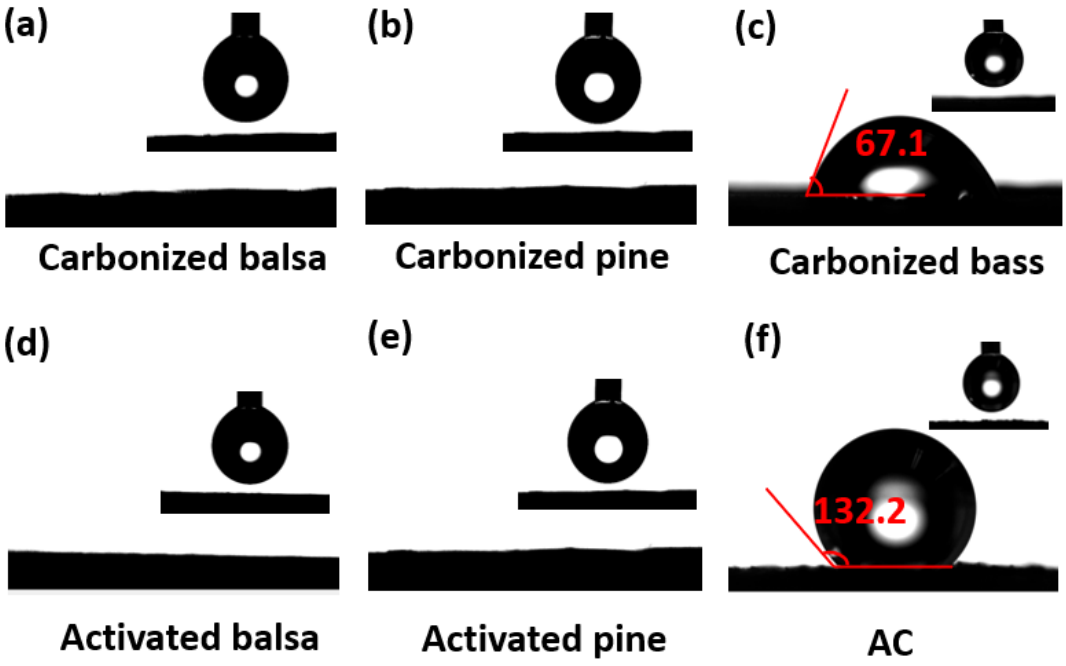

Figure 3. Water contact angle of carbonized balsa, carbonized pine, carbonized bass, activated balsa, activated pine, and AC.

2.1.3 Surface area and pore size distribution

As shown in **Figure 4a**, the N_2 adsorption/desorption curve of each sample is easily identified, from which carbonized bass has a type II hysteresis loop-contained isothermal plot, indicating a non-porous structure. Meanwhile, the slope of carbonized balsa, carbonized pine curve gain an increase tendency with the raise of P/P0 at the beginning of the plot, presenting type H4 curves while AC owns a H3 plot.[8,35] The area of hysteresis loops is further proved by Barrett-Joyner-Halenda (BJH) pore size distribution as shown in Figure 4b.[36] Carbonized balsa exhibits a curve

with multi-peaks among 1.1 nm to 5 nm, which demonstrates the appearance of micro (1.1-2 nm) and mesopores (2-50 nm); while carbonized pine and AC have an overall decrease curve from 1.1 nm to 3 nm, and pore size distribution after 3 nm pore width is less than 0.03 cm^3 g^{-1} nm^{-1} for carbonized pine sample, indicating micropores dominate the total porous structure. Carbonized pine and AC also show the existence of mesopores peaks at 3.9 and 3.8 nm, respectively. In our experiments, the smallest pore width measured is approximately 1nm, this is because for micropores with 1-2 nm pore size, the salt adsorption behavior could be explained by modified Donnan theory, which will be discussed in section 2.3.[7,21,37]

The SSA and pore volume are calculated in **Table 1**. Carbonized balsa owns 592.36 m^2 g^{-1} SSA regarding to Brunauer-Emmett-Teller (BET) method, with 105.01 m^2 g^{-1} micropore (<2 nm pore width) and 487.35 m^2 g^{-1} mesopore (>2 nm pore width) SSA. The large number of mesopores SSA confirms the result from the wide hysteresis loop area and pore size distribution. Likewise, carbonized pine and AC have more micropores than mesopores, and SSA are 687.96 and 787.94 m^2 g^{-1}, respectively. Surprisingly, carbonized bass shows an ultra-low SSA, 31.88 m^2 g^{-1}, reflected by the low isothermal and pore size distribution curve. This result may be caused by the block of channels as shown in Figure 2m red circle. The pore volume result is proportional to the SSA, where carbonized balsa, carbonized pine, and AC have 0.427, 0.372, and 0.707 cm^3 g^{-1}, respectively. Usually, a large SSA will lead to superior water deionization because a large surface area enables more contact area between the carbon electrode and ion-contained water.[21]

For activated wood converted carbon samples, the chemical reaction between KOH and carbon further forges supplementary pore structure and reinforces the SSA of the samples. As shown in Table 1, activated balsa shows an 808.74 m^2 g^{-1} SSA, with 281.72 m^2 g^{-1} micropore SSA and 527.02 m^2 g^{-1} mesopore SSA. Likewise, activated balsa owns an enhanced total SSA of 778.54 m^2 g^{-1}. After the activation, both micropore and mesopore SSA are increased, illustrating the creation of extra porous structure. However, activated balsa exhibits more increased SSA (216.38 m^2 g^{-1}) than activated pine (90.58 m^2 g^{-1}). To our understanding, this might be because the wall thickness of carbonized balsa is only approximately 200 nm while the carbonized pine owns more than 600 nm carbon wall thickness (Figure 2e and j). Thus, when activation occurs, the thin wall structure can be damaged by carbon-KOH reaction easily and create extra porous structure, while the morphology of thick carbon wall of carbonized pine is arduous to be modified (Figure S1).[38]

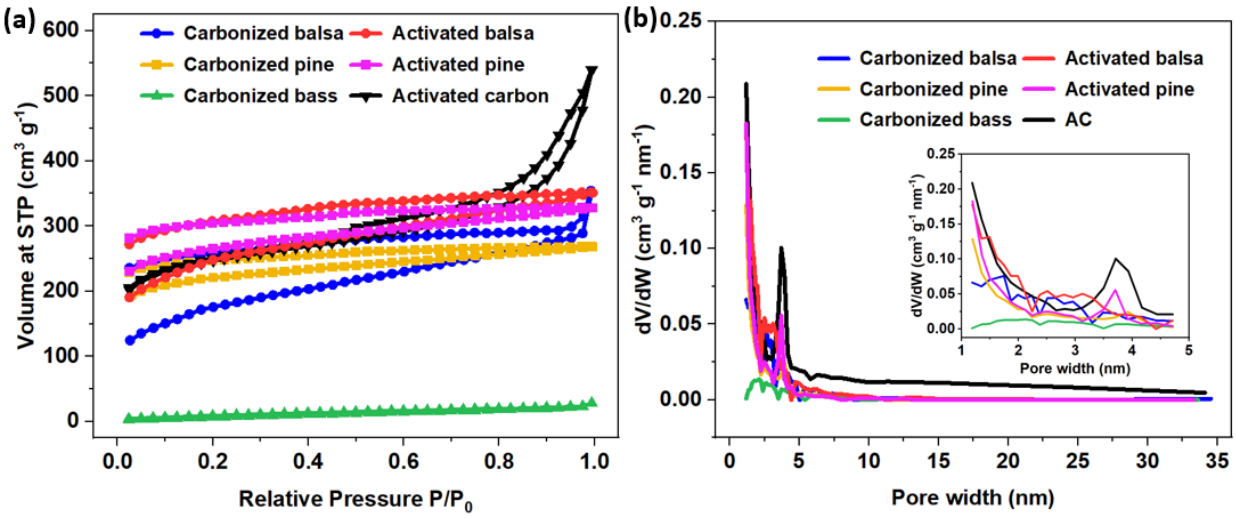

Figure 4. (a) N_2 adsorption/desorption isothermal and (b) BJH pore size distribution of carbonized balsa, carbonized pine, carbonized bass, AC, activated balsa and activated pine. Insert shows the pore size distribution of 1-5 nm pores.

Table 1. The specific surface area, electrical property and SAC summary of wood converted carbon and activated carbon samples

	S_{BET} [m^2 g^{-1}]	S_{micro} [m^2 g^{-1}]	S_{meso} [m^2 g^{-1}]	Specific capacitance at 2mV s^{-1} [F g^{-1}]	SAC [mg g^{-1}]
Carbonized balsa	592.36	105.01	487.35	69.90	5.27±0.61
Carbonized pine	687.96	449.77	238.19	83.21	5.47±0.25
Carbonized bass	31.88	0	31.88	3.42	0±0
AC	787.94	414.12	373.82	46.04	5.04±0.03
Activated balsa	808.74	281.72	527.02	102.48	12.45±1.64
Activated pine	778.54	512.14	279.66	87.04	6.99±0.44

2.2 Electrical property

Cyclic voltammetry (CV) analysis was applied to study the specific capacitance of carbon samples. The potential window was selected from -0.4 to 0.6 V, and sweep rates were from 2 mV/s to 200 mV/s. As shown in **Figure 5a**, at 2 mV s^{-1} scan rate, the quasi-rectangular shape curve appears without an obvious oxidation or reduction peak, indicating no faradaic reaction, but EDL occurs in most of carbon samples. A tiny redox peak is visible in carbonized and activated balsa samples,

indicating the appearance of oxidation. Carbonized pine has the most extensive curve area compared to the other three carbonized samples, which suggests a considerable capacitance (83.21 F g^{-1} at 2 mV s^{-1}). Moreover, carbonized balsa exhibits higher capacitance than AC, which are 69.90 F g^{-1} and 46.04 F g^{-1}, respectively. This is because the hydrophobic property of AC (section 2.1.2) prevents the access of salt ions to the internal of the AC electrode. Meanwhile, the marvelous hydrophilic property in NaCl solution retained in both carbonized balsa and carbonized pine provides a tight interaction between carbon and water molecules, which will benefit the ion transport and accelerate the ion diffusion rate.[32] The specific capacitance of activated balsa and activated pine are 102.48 and 87.04 F g^{-1}, respectively, regarding to Figure 5a. Obviously, all activated samples involve a surpassing capacitance compared to carbonized wood. Activated balsa occupies the highest specific capacitance among the three samples, illustrated by its enormous ion collision section afforded by high SSA. Compared to the other three carbon samples, carbonized bass shows extremely poor capacitance (3.42 F g^{-1} at 2 mV s^{-1}) as shown in both Figures 5a and b, which attribute to the tiny area of the EDL constituted through its low SSA. It is also noticeable that the specific capacitance decreases with an increasing scan rate (Figure 5b), which is caused by insufficient time for ions to access the EDL at a high scan rate.[39]

The Nyquist plots are provided in Figure 5c. At high frequency, a distinct semi-circle can be observed, the width of which demonstrates the charge transfer resistance (R_{ct}) of the samples. As can be identified, the R_{ct} of carbonized balsa, carbonized pine, and AC are 6.78, 12.62, and 18.22 Ω, respectively, while carbonized bass shows an ultra-large semi-circle diameter. The R_{ct} of activated balsa and pine are 17.51 and 13.40 Ω, respectively. Basically, a lower specific capacitance will result in a higher resistance.[30] However, it is noticeable that the resistance of activated wood converted carbon is higher than carbonized wood. This might be caused by the channel structure of the binder-free carbon electrode. After carbonization, the formation of pores and cracks further increase the transferring distance from the current collector to the electrode surface and thus limit the ion mobility inside the activated pore system. [21] Thus, the sequence of R_{ct} would be carbonized bass > AC > activated balsa > activated pine > carbonized pine > carbonized balsa. However, as observed in the galvanostatic charge-discharge (GCD) curve, the AC has the largest (4.03 V) while activated balsa shows the lowest (0.24 V) iR drop at 1A/g current density between 0-1V, indicating a low resistance of activated balsa samples (Figure 5d). The charge/discharge time for carbonized bass is too fast to be captured by the GCD curve, revealing

a low specific capacitance.[9] Above all, the electrochemical property of carbon samples is affected by the surface area and hydration property. Due to the high capacitance and low resistance, activated balsa is appropriate to be applied as electrodes for the deionization experiment.

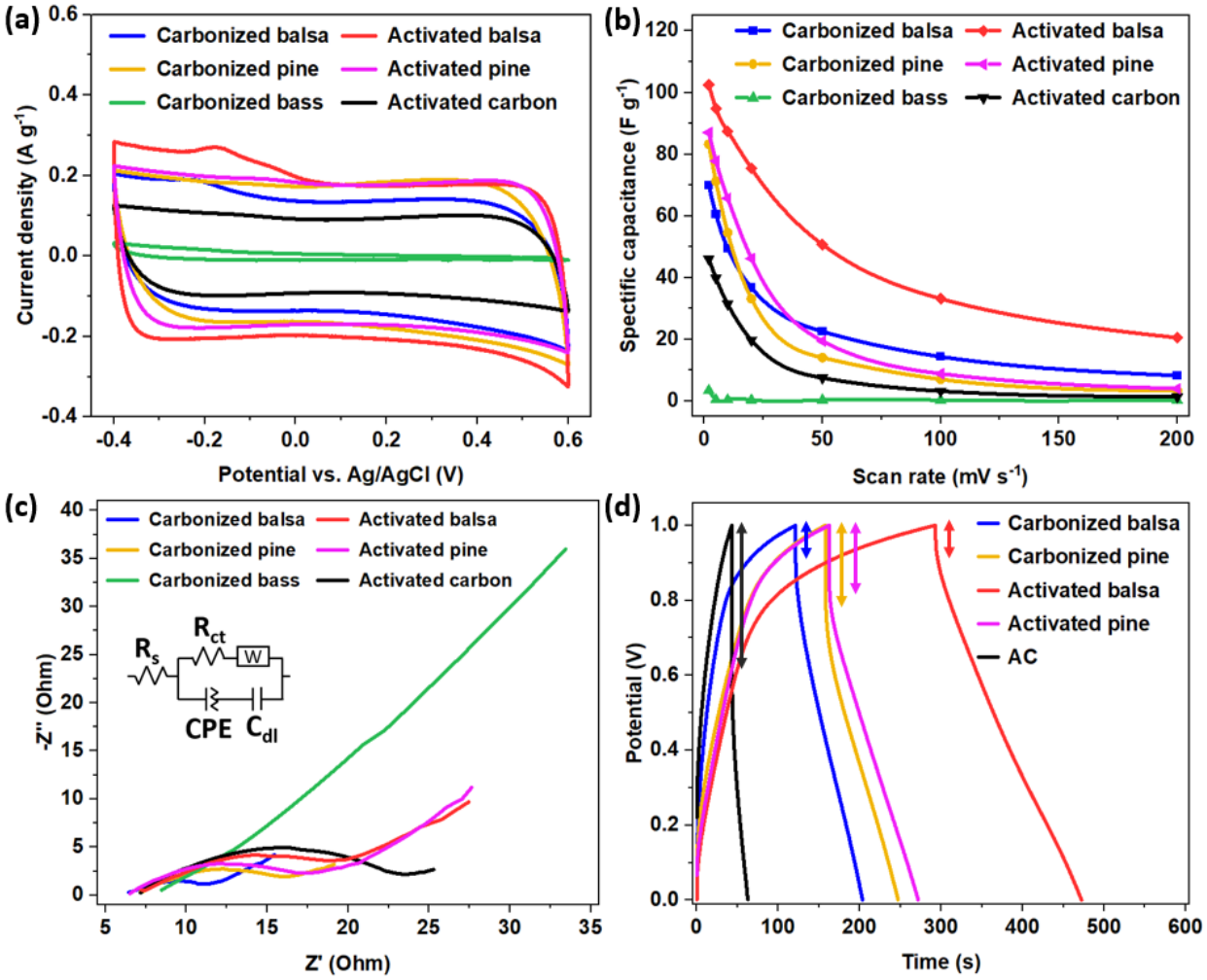

Figure 5. (a) CV curves of carbonized balsa, carbonized pine, carbonized bass, activated balsa, activated pine and AC at a sweep rate of 2 mV s^{-1}. (b) Specific capacitance at different scan rates. (c) EIS curve of carbon samples. (d) GCD curve at 1 A g^{-1} current density, arrow shows the iR drop. The sample size for electrical test is approximately 5mm*5mm*1mm.

2.3 Salt adsorption performance

Before the desalination experiment, the 500 ppm NaCl solution was pumped into the cell over 5 hours (without voltage applied) until the conductivity doesn't change to minimize the influence of physical adsorption of porous carbon electrodes on the final SAC results. The desalination was carried out under the 1.2 V voltage experimental condition to prevent the electrolytic action in a single-pass mode to mimic the real desalination process (**Figure 6a**). As shown in **Figure S3**, the conductivity of NaCl solution decreases dramatically during the first several minutes, indicating huge adsorption of NaCl ions and the formation of EDLs inside the carbon samples. The conductivity increases back to its initial level after 50 mins, illustrating the adsorption was accomplished. As shown in Figure 6b, carbonized balsa, carbonized pine, and AC have comparable SAC results, among them the best SAC was provided by carbonized pine, which is 5.47 mg g^{-1}, while carbonized balsa shows a 5.27 mg g^{-1} SAC, slightly higher than that of AC (5.04 mg g^{-1}). However, the conductivity curve of carbonized bass is a nearly straight line (Figure S3), which means no adsorption occurred. Among all tested samples, activated balsa has the highest NaCl adsorption capacity of 12.45 mg g^{-1}, while 50 mins charge period is insufficient for activated pine to accomplish the adsorption (Figure 6b), and the SAC of activated pine is 6.99 mg g^{-1} after 120 mins adsorption period (Figure S3). As shown in **Table 2**, to the best of our knowledge, this is so far the highest NaCl adsorption capacity performance by using wood converted carbon as electrode. Other than comparing with the existing wood converted carbon materials, our SAC is also exceptional to other biomass converted carbon, shown in Table 2.[10,13,15,30,40–42] Figure 6d illustrates CDI performance under several adsorption/desorption cycles using activated balsa as the electrode, during which there is no obvious decline of the SAC. It is also noticeable that after more than 12 hours salt adsorption, we did not observe any significant morphology changes (Figure S4), demonstrating that activated balsa exhibits a robust structure to obtain a stable NaCl adsorption performance. According to the Ragone plot as shown in Figure 6c, activated balsa curve is located at the top and right regions, demonstrating the activation process contributes to a faster salt adsorption rate and higher SAC.[43] The excellent SAC and proportionate average salt adsorption rate (ASAR) result shown by the activated balsa contributed to the enormous surface area and generous specific capacitance. In summary, activated balsa performances as an excellent CDI electrode material for NaCl adsorption.

Table 2. List of SAC results from other works

Electrode materials	CDI mode	Brackish water concentration	Voltage [V]	SAC [mg g^{-1}]	Ref
Activated balsa	Single-pass	500 mg L^{-1} NaCl	1.2	12.45	**This work**
Leucocephala wood converted carbon	Batch	0.5 mM NaCl	1	2.1	[40]
Bass wood converted carbon	Batch	100 mg L^{-1} NaCl	1.2	5.7	[15]
Cotton converted carbon	Batch	500 mg L^{-1} NaCl	1.2	4.9-16.1	[30]
Lentinus edodes converted carbon	Batch	500 mg L^{-1} NaCl	1.2	12.9	[42]
Activated biochar	Batch	500 mg L^{-1} NaCl	1.2	5.07-5.39	[41]
Citrus peels converted carbon	Batch	500 mg L^{-1} NaCl	1.5	5.22-10.79	[10]
Xylose converted carbon	Batch	1000 mg L^{-1} NaCl	1.2	16.29	[13]

To deeply understand the salt adsorption kinetics, the biomass converted electrodes have been systematically characterized and studied with the existing theories: (1) SSA: In general, high surface area is one of the preeminent aspects that ensures the exceptional salt adsorption. Due to the formation of EDLs between the surface of carbon and NaCl solution during charge process, an immense EDLs area capable of attracting substantial ions.[44] In our experiments, the surface area of the electrode largely dependent on the natural wood's original morphology. The outstanding porous structure owned by carbonized balsa and pine electrodes ensure the over 5 mg g^{-1} SAC result. While the blocked channel negatively decreases the SSA of carbonized bass wood (31.88 m^2 g^{-1}), the electrodes exhibit limited EDLs and we did not observe any noticeable adsorption performance (0 mg g^{-1}). Moreover, taking advantages of the extra porous structures created by the KOH-carbon reaction, the activated balsa displays enlarged SSA (808.74 m^2 g^{-1}) and leading to the superior SAC (12.45 mg g^{-1}). Furthermore, activation is an applicable approach to enlarge the SSA and enhance the salt adsorption performance for other kinds of wood. For example, activated balsa shows 216.38 m^2 g^{-1} extra SSA. Activated pine only has less than 100 m^2 g^{-1} SSA created by chemical reaction between carbon and KOH, which is due to difference from the carbon wall thickness as discussed in section 2.1.3. Therefore, not all of wood converted carbons will be ideal to be utilized in CDI, though most are applicable. (2) Pore-size distribution: Helmholtz and Gouy-

Chapman-Stern (GCS) theory are the two initial models that help explaining the EDLs kinetics.[45,46] A stern layer that adhere to the charged carbon, full of oppositely charged ions, and a diffuse layer, in which the ion concentration declines with a further distance from the electrode occur.[21] However, both models are not sufficient to clarify the EDLs kinetics in micropore structures.[20] Thus, modified Donnan (mD) model provides the theoretical guidance on overlapped diffuse layers in micropore structures, which is more appropriate in implying the EDLs in micropores.[47] Therefore, the overlapped diffuse layer assists revealing the adsorption kinetics in micropores (<2 nm pore width) and GCS model is appropriate for mesopore (>2 nm pore width) adsorption. Based on our experimental results, both micro- and meso- pore structure endure in carbonized and activated wood. For example, carbonized pine and activated pine surface area results imply that over 65% of SSA belong to micropore (Table 1), in which the Debye length is larger than pore width and EDLs are overlapped.[21] While for carbonized balsa and activated balsa, the mesopore dominate the total SSA result, indicating largely appeared mesopore adsorption exists on both the surface of the electrode (if the EDLs are not overlapped) and inside pore volume (if EDLs are partially overlapped). The analogous SAC results of carbonized balsa (meso-dominated) and pine (micro- dominated) (5.24 and 5.47 mg g^{-1}) demonstrate that both micro- and meso-pore play a critical role in salt adsorption performance. After activation, both activated balsa and pine imply approximately 40 m^2 g^{-1} increase in mesopore SSA, and micropore SSA of activated balsa largely increased, leading to a superior SAC to activated pine (Table 1). In summary, by selecting convenient natural wood and employing the activation process to prepare the biomass carbon, we are able to control the micro- and meso- porous structure in nano level, further to control the EDLs performance during adsorption process. (3) Surface properties: Surface hydration and energy determine the interaction between brackish water and carbon electrode. A hydrophilic electrode and high surface energy ensure a strong interconnection between NaCl solution and carbon. Thus, once the electrode immersed into the solution, the water contains the ions will fulfill the entire part of the electrode. During the charge process, the ions can move towards carbon and form EDLs without air barriers. In our biomass materials, both carbonized wood samples exhibit the hydrophilic properties while balsa and pine carbon samples show the extraordinary 0 degree water contact angle with 82.23 mN m^{-1} surface energy. This is because of the surface morphology of the carbon samples promote the water penetration as discussed in section 2.1.2. Meanwhile, due to the addition of polymer binder, the AC films display a

hydrophobic property, indicating that the internal of AC may not be able to participate in the adsorption, which wastes some of the EDLs area and unfortunately prevent the ions' adsorption.[21] As a result, the natural wood structure that retained in carbonized wood benefits the formation of super hydrophilic performance, and the binder-free wood converted carbons are the applicable candidate as the CDI electrode. (4) Electrical properties: The electrical properties of the electrode also play a critical role in desalination performance. Due to the electrochemical adsorption kinetic characteristic owned by carbon electrode in CDI, the specific capacitance of the electrode directly reflects salt adsorption performance. The charge and discharge period are when the electrolyte ions being absorbed and released by carbon electrode.[48] Generally speaking, the high specific capacitance indicates the massive ion diffusion between the NaCl and carbon electrode.[21,49] Due to the large area of EDLs between the electrolyte and electrode, the electrode owns higher surface area usually shows better specific capacitance, and our experimental results follow this rule as well. The activated balsa owns the highest SSA (808.74 $m^2 g^{-1}$) and specific capacitance at 2mV s^{-1} scan rate (102.48 F g^{-1}) at the same time. This extraordinary result comes from the widespread stern and diffuse layers that attract the electrolyte ions to the surface of the electrode. Moreover, the low resistance of carbonized pine, carbonized balsa, activated pine and activated balsa (Table 1) ensure no significant voltage degradation during the charging process within the device. Thus, the strong electrostatic force between electrode and salt ions benefits the formation of EDLs, results in a high SAC performance.[21]

In addition to NaCl desalination, activated balsa converted carbon electrode has a great potential in heavy metal adsorption, based on its outstanding performance in CDI tests. We performed heavy metal ion adsorption on activated balsa under 1.2 V with 100 ppm $PbCl_2$ and 50 ppm $CrCl_3$ brackish water, respectively, in batch mode. As shown in Figure 6e, the adsorption capacity for Pb^{2+} and Cr^{3+} are 19.52 and 20.06 mg g^{-1}, respectively, which indicates activated balsa owns an excellent heavy metal adsorption performance which is comparable to other's work.[31,50] It has been proved widely by others that the higher initial concentration of brackish water will result in a better SAC result due to the enriched mass transfer rate.[51,52] Thus, a conclusion can be cautiously drawn that the ions adsorption capacity of activated balsa is $Cr^{3+} > Pb^{2+} > Na^{+}$. This is because Cr^{3+} ions have an excessive valence, while the charge size for Pb and Na ions are 2+ and 1+, respectively. The enriched valence provokes a robust electrostatic force between the ions and carbon electrode, and thus Cr^{3+} is more favorable to be absorbed.[53]

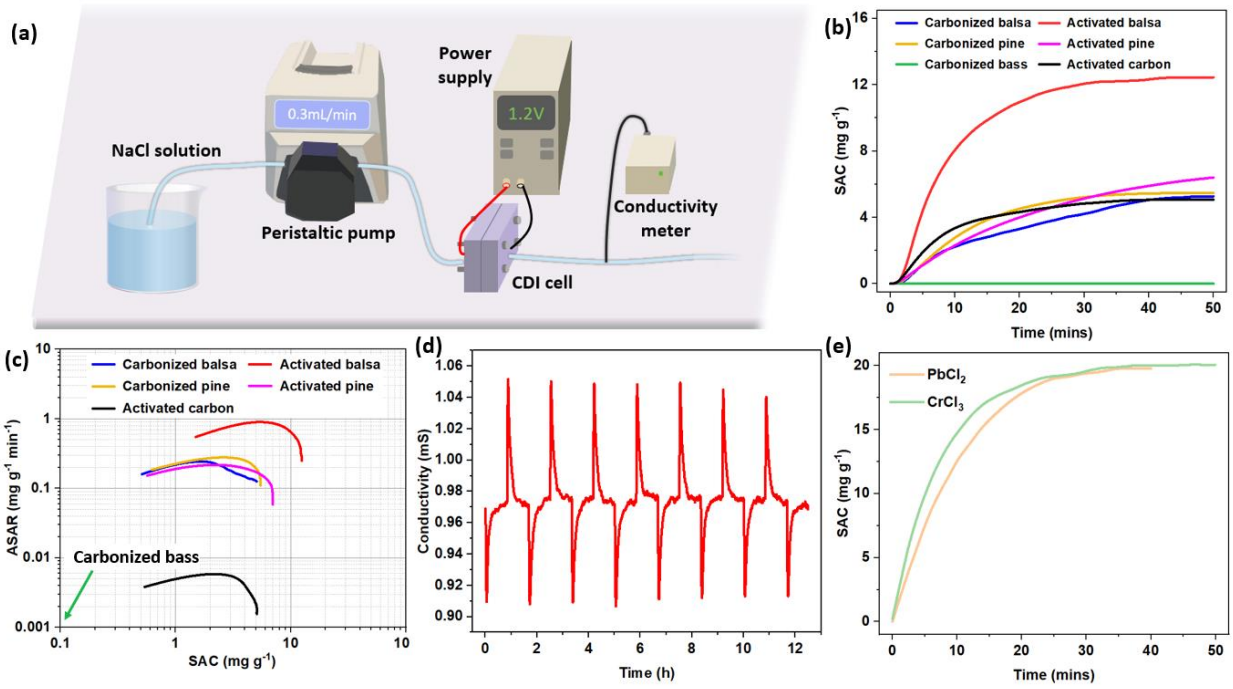

Figure 6. Water desalination performance. (a) NaCl adsorption experimental setup. (b) SAC summary of NaCl adsorption. (c) Ragone plot of carbonized and activated wood samples (d) Multi-cycles salt adsorption performance of activated balsa. (e) Heavy metal adsorption of activated balsa. The sample size for salt adsorption is 8mm*8mm*1mm.

3. Conclusion

As a green approach, this work has successfully demonstrated the feasibly of using biomass materials to enable high-performance CDI devices by systematically study the materials properties and adsorption kinetics. The binder-free wood converted carbon has been successfully synthesized from balsa, pine, and bass wood, in which the natural wood porous structure was maintained. Among three-carbon materials, carbonized balsa and carbonized pine possess a large surface area and good specific capacitance, leading to a decent NaCl adsorption performance. The further KOH activation on carbonized wood creates more porous structures. Activated balsa shows the 12.45 mg g^{-1} SAC, which is so far the highest SAC reported by using wood converted carbon as CDI electrode. The extraordinary result is more than twice as activated carbon due to high surface area and excellent electrical property of activated balsa converted carbon. Additionally, activated balsa

shows an extraordinary heavy metal adsorption performance. The SAC for Pb^{2+} and Cr^{3+} are 19.52 and 20.06 mg g^{-1}, respectively. As there is a lot of biomass generated each year, converting biomass to the electrode materials of energy-efficient high-performance water desalination device could pave a new way to pursue a sustainable society in the future.

4. Experimental Section/Methods

Carbonized wood preparation: The natural-grown balsa, pine, and bass wood were cut into sheet pieces, vertical to the growth direction. The moisture inside the wood pieces was depleted by drying the samples in the oven for 6 hours. Once dried, the samples were transferred into a tube furnace. The carbonization occurred at 1000 ^{o}C for 6 hours with Ar as protection gas. After the temperature cooled down, the samples were taken out and polished with sandpaper to flatten the surface. Then, the wood converted carbon pieces were immersed into deionized (DI) water and ethanol several times to eliminate the surplus, tiny debris from pores, during which an ultrasonicate process was applied. When the liquid appeared transparent after sonication, the samples were taken out and placed into the oven at 120 ^{o}C for 4 h. The three wood converted carbon samples were named carbonized balsa, carbonized pine, and carbonized bass. It is noticeable that the different positions of the wood may have significant variable structures. Therefore, all the samples were chosen from same dense area.

Activated wood converted carbon preparation: The obtained balsa and pine converted carbon pieces were immersed in 5mol L^{-1} KOH solution for 30 hours, after which the samples were dehydrated in the oven at 80 ^{o}C overnight. Afterward, the samples were placed inside a tube furnace for activation. The temperature was increased to 700 ^{o}C within the first 30 minutes, followed by 2 hours activation at the constant targeted temperature. The whole process was under N_2 protection. When the temperature cooled down to room temperature, the activated wood converted carbon pieces were neutralized with 20% HNO_3 solution and washed with DI water. Finally, the samples were dried in the oven and stored for further characterization. The activated samples were named activated balsa and activated pine respectively.

Activated carbon film preparation: AC film was tagged as a comparison group and prepared by solution casting method. The AC powder (Sigma-Aldrich, 100 mesh particle size) was added into

a polymer binder solution consisting of polyvinylidene fluoride (PVDF) and dimethylformamide (DMF). The total amount of PVDF binder was 5% to AC powder. A vigorous stirring was conducted to ensure a thorough mixture, during which extra DMF was added to adjust the viscosity of the mixture until the carbon slurry was obtained. Then, the slurry was transferred onto a polytetrafluoroethylene (PTFE) substrate placed above an 80 ^{o}C hotplate. The carbon film was collected after an overnight DMF evaporation.

Material characterization: A scanning electron microscope (SEM, JOEL JSM-IT500HR) was applied to observe the morphology of the carbon samples. The N_2 adsorption/desorption (Anton Paar, autosorb iQ) was applied for the porosity of the samples, in which the Brunauer-Emmett-Teller (BET) method was utilized for surface area and the Barrett-Joyner-Halenda (BJH) method was used for pore size distribution. The surface area of micropores was calculated by t-plot analysis. The hydration property was tested through water contact angle by goniometer (Dataphysics, OCA 15EC).

Electrochemical characterization: An electrochemical workstation (CHI 660e) was utilized to test the electrical properties of samples through a three-electrode system, which consists of an Ag/AgCl reference electrode, a Pt counter electrode, and carbon sample as a working electrode. The electrodes were immersed in 1M NaCl solution during the experiment. The specific capacitance was calculated through the cyclic voltammetry (CV) curve and by the equation:

$$C = \frac{\int I\,dV}{2vm\Delta V} \quad (3)$$

Where C represents the specific capacitance, I represents the current, V represents the potential, v represents the scan rate, m represents the mass of electrode, and ΔV is the potential window.

In addition, electrochemical impedance spectroscopy (EIS) and galvanostatic charge-discharge (GCD) were tested under the duplicated condition.

NaCl deionization: Single-pass mode was applied for the NaCl deionization experiment. A pair of carbon electrodes approximately the size of 1cm×1cm was installed into a 3D printed CDI cell, followed by covering with ion-exchange members (IEMs). A single layer of net separator was placed between two IEMs to prevent an internal short circuit. 500 ppm NaCl solution was prepared and pumped into the sealed CDI cell by a peristaltic pump with a 0.3 mL min^{-1} flow rate. The

outlet of the CDI cell was connected to a flow-through conductivity meter (eDAQ, isopod). The final SAC and ASAR were calculated by the equations below:

$$SAC = \frac{\int (C_0 - C)\, dt\, vt}{m} \quad (4)$$

$$ASAR = \frac{SAC}{t} \quad (5)$$

Where C represents the concentration of NaCl flowing out of CDI cell, C_0 represents the initial NaCl concentration (500 ppm), t represents the time, v represents the flow rate, m represents the mass of the carbon electrodes.

Heavy metal deionization: Batch mode was applied for heavy metal deionization. The CDI cell installation is the same as the NaCl deionization method. 100 ppm $PbCl_2$ and 50 ppm $CrCl_3$ were prepared as brackish water. The ion contained liquid, with a total volume 20 mL, was pumped into the CDI cell and flowed back with a 5 mL min^{-1} speed. The concentration of heavy metal ions was measured by a conductivity meter (eDAQ, isopod) inserted into the liquid. The SAC was calculated by the equation:

$$SAC = \frac{(C_0 - C)V}{m} \quad (6)$$

Where V is the total volume of heavy metal solution.

Statistical Analysis

The SAC results shown in Table 1 are the mean ± standard deviation (SD) from at least three adsorption tests. N_2 adsorption/desorption, pore size distribution, CV and GCD curves are the raw data of one test directly read from the instrument. All curves are plotted by Origin software.

Supporting Information

Supporting Information is available from the Wiley Online Library or from the author.

Acknowledgement

P. D. and Y. Yang acknowledge the financial support from the Department of the Interior, Bureau of Reclamation under contract R19AC00116. P.D acknowledges the financial support from 4VA.

Conflict of Interest

The authors declare no conflict of interest.

Reference

[1] I. Ghosh, Visualizing the total biomass of every animal on Earth, https://www.weforum.org/agenda/2021/08/total-biomass-weight-species-earth, accessed: August, **2015**.

[2] J. Shelly, P. Tittmann, S. Mohammadi, *Woody Biomass Factsheet–WB1*, https://www.pelletheat.org/assets/docs/industry-data/infoguides43284.pdf, accessed: Feburary, **2016**.

[3] X. Hong, R. Wang, Y. Liu, J. Fu, J. Liang, S. Dou, *J. Energy Chem.* **2020**, *42*, 144.

[4] J. Wang, X. Zhang, Z. Li, Y. Ma, L. Ma, *J. Power Sources* **2020**, *451*, 227794.

[5] M. B. Ahmed, M. A. Hasan Johir, J. L. Zhou, H. H. Ngo, L. D. Nghiem, C. Richardson, M. A. Moni, M. R. Bryant, *J. Clean. Prod.* **2019**, *225*, 405.

[6] P. Kalyani, A. Anitha, *Int. J. Hydrogen Energy* **2013**, *38*, 4034.

[7] L. Han, K. G. Karthikeyan, M. A. Anderson, K. B. Gregory, *J. Colloid Interface Sci.* **2014**, *430*, 93.

[8] D. Xu, Y. Tong, T. Yan, L. Shi, D. Zhang, *ACS Sustain. Chem. Eng.* **2017**, *5*, 5810.

[9] S. Zhao, T. Yan, Z. Wang, J. Zhang, L. Shi, D. Zhang, *RSC Adv.* **2017**, *7*, 4297.

[10] Z. Xie, X. Shang, J. Yan, T. Hussain, P. Nie, J. Liu, *Electrochim. Acta* **2018**, *290*, 666.

[11] C. Zhao, S. Zhang, N. Sun, H. Zhou, G. Wang, Y. Zhang, H. Zhang, H. Zhao, *Environ. Sci. Water Res. Technol.* **2019**, *5*, 1054.

[12] M. S. Gaikwad, C. Balomajumder, *Chemosphere* **2017**, *184*, 1141.

[13] T. Lu, Y. Liu, X. Xu, L. Pan, A. A. Alothman, J. Shapter, Y. Wang, Y. Yamauchi, *Sep. Purif. Technol.* **2021**, *256*, 117771.

[14] J. H. Choi, *Sep. Purif. Technol.* **2010**, *70*, 362.

[15] M. Liu, M. Xu, Y. Xue, W. Ni, S. Huo, L. Wu, Z. Yang, Y.-M. Yan, *ACS Appl. Mater. Interfaces* **2018**, *10*, 31260.

[16] H. T. El-Dessouky, H. M. Ettouney, Y. Al-Roumi, *Chem. Eng. J.* **1999**, *73*, 173.

[17] Y.-M. Chao, T. M. Liang, *Desalination* **2008**, *221*, 433.

[18] L. F. Greenlee, D. F. Lawler, B. D. Freeman, B. Marrot, P. Moulin, *Water Res.* **2009**, *43*, 2317.

[19] Y. H. Teow, A. W. Mohammad, *Desalination* **2019**, *451*, 2.

[20] M. E. Suss, S. Porada, X. Sun, P. M. Biesheuvel, J. Yoon, V. Presser, *Energy Environ.*

Sci. **2015**, *8*, 2296.

[21] S. Porada, R. Zhao, A. Van Der Wal, V. Presser, P. M. Biesheuvel, *Prog. Mater. Sci.* **2013**, *58*, 1388.

[22] Y. J. Chen, C. F. Liu, C. C. Hsu, C. C. Hu, *Electrochim. Acta* **2019**, *302*, 277.

[23] V. Pothanamkandathil, C. A. Gorski, *Environ. Sci. Water Res. Technol.* **2022**, *8*, 1489.

[24] Y. Oren, *Desalination* **2008**, *228*, 10.

[25] A. T. Angeles, J. Lee, *Chem. Rec.* **2021**, *21*, 820.

[26] S. D. Datar, R. Mane, N. Jha, *Water Environ. Res.* **2022**, *94*.

[27] J. Wang, S. Kaskel, *J. Mater. Chem.* **2012**, *22*, 23710.

[28] G. E. Harimisa, N. W. C. Jusoh, L. S. Tan, K. Shameli, N. A. Ghafar, A. Masudi, *J. Phys. Conf. Ser.* **2022**, *2259*.

[29] A. Hai, G. Bharath, K. R. Babu, H. Taher, M. Naushad, F. Banat, *Process Saf. Environ. Prot.* **2019**, *129*, 103.

[30] G. X. Li, P. X. Hou, S. Y. Zhao, C. Liu, H. M. Cheng, *Carbon N. Y.* **2016**, *101*, 1.

[31] R. Chen, T. Sheehan, J. L. Ng, M. Brucks, X. Su, *Environ. Sci. Water Res. Technol.* **2020**, *6*, 258.

[32] C. Kim, J. Lee, S. Kim, J. Yoon, *Desalination* **2014**, *342*, 70.

[33] D. Janssen, R. De Palma, S. Verlaak, P. Heremans, W. Dehaen, *Thin Solid Films* **2006**, *515*, 1433.

[34] N. L. Liu, S. H. Sun, C. H. Hou, *Sep. Purif. Technol.* **2019**, *215*, 403.

[35] M. Thommes, K. Kaneko, A. V Neimark, J. P. Olivier, F. Rodriguez-Reinoso, J. Rouquerol, K. S. W. Sing, *Pure Appl. Chem.* **2015**, *87*, 1051.

[36] R. Bardestani, G. S. Patience, S. Kaliaguine, *Can. J. Chem. Eng.* **2019**, *97*, 2781.

[37] Y. Zhang, P. Ren, Y. Liu, V. Presser, *Desalination* **2022**, *525*, 115503.

[38] Z. Li, W. Lv, C. Zhang, B. Li, F. Kang, Q. H. Yang, *Carbon N. Y.* **2015**, *92*, 11.

[39] X.-L. Su, M.-Y. Cheng, L. Fu, J.-H. Yang, X.-C. Zheng, X.-X. Guan, *J. Power Sources* **2017**, *362*, 27.

[40] C. H. Hou, N. L. Liu, H. C. Hsi, *Chemosphere* **2015**, *141*, 71.

[41] A. M. Dehkhoda, N. Ellis, E. Gyenge, *Microporous Mesoporous Mater.* **2016**, *224*, 217.

[42] J. Yan, H. Zhang, Z. Xie, J. Liu, *AIP Conf. Proc.* **2017**, *1864*, 020218.

[43] T. Kim, J. Yoon, *RSC Adv.* **2015**, *5*, 1456.

[44] Y. Liu, C. Nie, X. Liu, X. Xu, Z. Sun, L. Pan, *RSC Adv.* **2015**, *5*, 15205.

[45] M. E. Suss, T. F. Baumann, W. L. Bourcier, C. M. Spadaccini, K. A. Rose, J. G. Santiago, M. Stadermann, *Energy Environ. Sci.* **2012**, *5*, 9511.

[46] R. Zhao, P. M. Biesheuvel, H. Miedema, H. Bruning, A. van der Wal, *J. Phys. Chem. Lett.* **2010**, *1*, 205.

[47] P. M. Biesheuvel, R. Zhao, S. Porada, A. van der Wal, *J. Colloid Interface Sci.* **2011**, *360*, 239.

[48] H. Hu, Z. Pei, C. Ye, *Energy Storage Mater.* **2015**, *1*, 82.

[49] C. Yan, L. Zou, R. Short, *Desalination* **2012**, *290*, 125.

[50] T. Alfredy, Y. A. C. Jande, T. Pogrebnaya, *J. Water Reuse Desalin.* **2019**, *9*, 282.

[51] W. Shi, H. Li, X. Cao, Z. Y. Leong, J. Zhang, T. Chen, H. Zhang, H. Y. Yang, *Sci. Rep.* **2016**, *6*, 1.

[52] J. Oladunni, J. H. Zain, A. Hai, F. Banat, G. Bharath, E. Alhseinat, *Sep. Purif. Technol.* **2018**, *207*, 291.

[53] Z. Huang, L. Lu, Z. Cai, Z. J. Ren, *J. Hazard. Mater.* **2016**, *302*, 323.